Engineering Science and Technology, an International Journal 24 (2021) 974–989

HOSTED BY

Contents lists available at ScienceDirect

Engineering Science and Technology, an International Journal

journal homepage: www.elsevier.com/locate/jestch

Full Length Article

Effect of Co addition on microstructure and mechanical properties of new generation 3Cr-3W and 5Cr-3W steels

Gökhan Arici [a], Mustafa Acarer [a,*], Mesut Uyaner [b]

[a] Selçuk University, Department of Metallurgical and Materials Engineering, Technology Faculty, Konya 42075, Turkey
[b] Necmettin Erbakan University, Department of Aeronautical Engineering, Faculty of Aviation and Space Sciences, Konya 42140, Turkey

ARTICLE INFO

Article history:
Received 10 August 2020
Revised 24 November 2020
Accepted 27 December 2020
Available online 26 January 2021

Keywords:
Low Cr steels
Cobalt
Heat treatment
Mechanical properties
Microstructure
Notch toughness

ABSTRACT

In this study, the effect of Cr and Co on microstructure and mechanical properties of low Cr-W steels was investigated. For this goal, 3% Cr-3%W and 5% Cr-3%W steels, this may be an alternative to new generation low Cr steels, containing 0%, 0.5%, 1.5%, 3%, 4.5% Co, produced by casting and hot rolling. The samples were annealed at 1100 °C for 1 h, followed by quenching in air and tempering for 2 h at 710 °C. Ferrite, bainite, and martensite phases were determined in various volume fractions according to the chemical composition. Carbides precipitated within the grain and grain boundaries during tempering. Co bearing caused an increase of A1, A3, and Curie temperatures. Co slightly increased hardness and strength in both 3 Cr and 5 Cr alloys. However, the hardness and strength of 5 Cr alloys with all Co ratios were almost same that of 3 Cr alloys. The Charpy-V impact energies of 5 Cr steel are lower than 3 Cr steel with the same Co amount. The addition of Co up to 1.5% in steels with 3 Cr did not make any major changes in the notch toughness. However, the addition of 3% Co to the alloy significantly reduced impact energy. In 5 Cr steel, notch toughness generally decreased with the increase of Co amount.

1. Introduction

Main goals in energy production are to work with higher-efficiency and lower-cost. The higher efficiency is possible with materials that can operate at high temperatures and steam pressures with maximum life under these conditions. Working at high temperatures and steam pressure, reduces CO_2 emissions. Cr-Mo steels are one of the materials which are developed for these conditions. Cr-Mo steels, which are symbolized as P22, P91, P92, according to ASTM A335 standard and T22, T91, T92, according to ASTM A213 standard, are widely used in boilers, pipes, and tubes in power plants [1]. The steel used in the power plants in the early 1900 s has experienced significant developments over time, and in the 1980s, advanced steels that could be described as modern began to be produced. Then, changes in the amounts of alloying elements of these steels were made, or new alloying elements additions to these steels were begun to use to increase the lifetime and productivity and to decrease wall thickness and cost of tubes [1,2]. Within the scope of new developments, Mo is replaced by W; Nb is replaced by Ta; Ni replaced by Co; the amount of Cr and other alloying elements were changed [3,4]. Fig. 1 expresses the evolution of steam turbine efficiency as a function of steam temperature and steam pressure by years [5].

The nickel acts as an austenite stabilizer element for Cr-Mo (W) steels. Co is an austenite stabilizer element that can be used substitute for Ni and provides some advantages over Ni. Also, Co does not reduce the A1 and A3 temperatures, which are essential for heat treatment for these steels, unlike Ni [6]. Tempering at higher temperatures, which decreases the duration of heat treatment, provides an essential contribution to the formation of carbide and nitride. Co improves the strength and hardness and creep resistance according to the literature [7,8]. Co increases the carbon activation, so it increases the tendency of alloying elements to form carbides [7–9]. In addition to this, Co goes up the Curie temperature, which helps to retard diffusion [10].

There are many studies for Cr-Mo or Cr-W steels and their weld metal in the literature [1–5]. However, attempts for the effect of Co on low alloy Cr-W steels are limited in the literature [11,12] yet. Therefore, in this study, microstructures and mechanical properties of Fe-3Cr-3W and Fe-5Cr-3W steels that are described as low Cr-W steels with different ratios of Co were investigated.

* Corresponding author.
E-mail addresses: arici@selcuk.edu.tr (G. Arici), macarer@selcuk.edu.tr (M. Acarer), muyaner@selcuk.edu.tr (M. Uyaner).

Peer review under responsibility of Karabuk University.

https://doi.org/10.1016/j.jestch.2020.12.025
2215-0986/

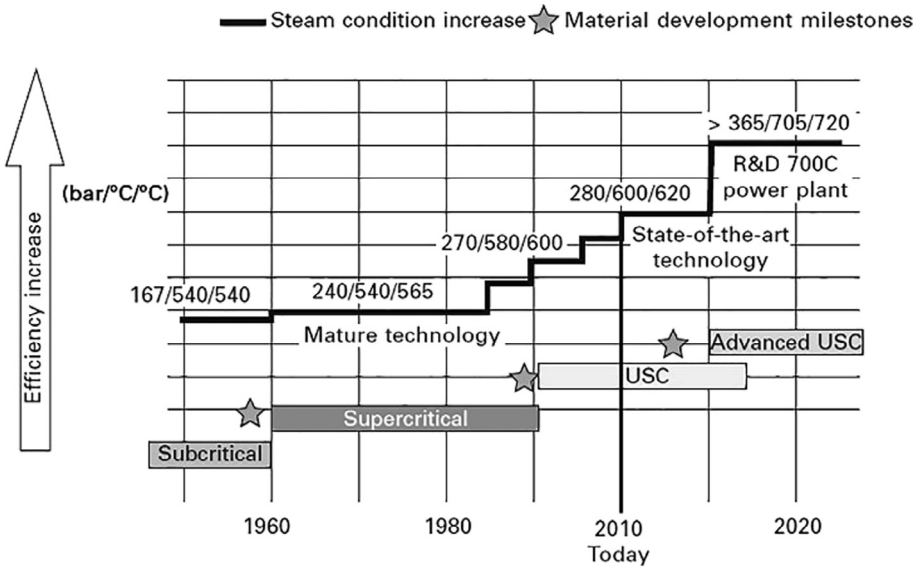

Fig. 1. The evolution of steam turbine operating conditions [5].

2. Experimental procedure

2.1. Material

Alloys were produced with dimensions of 17 mm × 26 mm × 275 mm by the investment casting method in this study. Fig. 2 shows the performed process. Table 1 summarizes the chemical composition of the as-cast steels (in wt. %). The casting process was carried out at 1600 °C and in an open atmosphere. Thickness of the samples reduced from 17 mm to approximately 3.5–4 mm by rolling at 1150 °C following casting.

2.2. Microstructural and structural characterizations

Cr-Mo (W) steels obtain the desired microstructural and mechanical properties via annealing and tempering heat treatments. Thermal analysis was performed in order to determine A1, A3, and the Curie temperatures of the samples under argon atmosphere from 25 °C to 1000 °C with a heating rate of 40 °C/min by using Hitachi STA 7300 TGA/DTA equipment. The samples were annealed at 1100 °C for 1 h according to temperatures, which determined by DTA analysis and then air-quenched. They were then tempered at 710 °C for 2 h. After annealing and tempering heat treatment, the samples were prepared for metallographic examination. They were ground with 180 up to 2000 grit silicon carbide paper and polished with 3 μm diamond paste. Then, samples were etched with picral (5 g picric acid + 100 ml ethyl alcohol) and LePera etchant. The optical microstructure examination was done by using Nikon MA 100 Eclipse optical microscope. The volume fractions of formed phases were estimated by using image analysis software (ImageJ 1.53f).

Scanning electron microscope (SEM) was used to image and determine the precipitates (carbide, nitride) formed after heat treatment. Energy-dispersive X-ray spectroscopy (SEM-EDS) was used to identify the elemental composition of precipitates. Chemical compositions of carbides were obtained after carbide precipitation have also been determined by SEM-EDS analysis. Zeiss Evo LS 10 microscope used for SEM and SEM-EDS analyses. In SEM and SEM-EDS analyzes, the samples prepared for optical metallographic investigations were characterized.

XRD analysis was performed for the identification of precipitates formed with a diffractometer with CuKα radiation over 2θ angles of 20 – 90° with a step size of 0.05. It is not possible to identify the precipitates of bulk samples by using XRD since the volume fraction of carbides is very low compared to the bulk sample. Therefore, the carbide extraction technique was used to identify the precipitates formed in each alloy. The carbide and/or nitrides were extracted by chemical dissolution of the ferrite in the electrolyte consisting of 10 vol% HCl in ethanol under 3 A current and 7 V voltage. XRD analysis was performed by Bruker D8 Advance X-ray diffractometer.

The morphology of the precipitates obtained by the carbide extraction was determined by the transmission electron microscope (TEM). The chemical composition of the precipitates was determined by TEM-EDS surface analysis. The precipitates were subjected to centrifuge process via ultrasonic cleaner in ethyl alcohol before TEM analyze. TEM and TEM-EDS analyses performed by using JEOL JEM-2100F field-emission transmission electron microscope operated at 200 kV.

2.3. Mechanical characterizations

Hardness, tensile, and Charpy-V impact tests were performed at room temperature to determine the effect of the amount of Cr and Co to hardness, tensile properties, and notch toughness, respectively. Hardness measurements of samples were performed at least five times at room temperature by using Bulut Digirock RBOV hardness tester with a 2.5-mm diameter steel ball and 187.5 kg load. Tensile test specimens were prepared proportionally to ASTM E8 (Fig. 3). Tensile tests were performed by using the Shimadzu AG-Xplus trade mark with 100 kN capacity. V-notch impact tests were carried out by using Alşa ZBC 2000 impact tester with 300 J capacity. Since the rolled thickness of samples (3.5 mm) is smaller than the thickness of the standard sample (10 mm according to ASTM E23-16b), results of measurement of notch impact tests are calculated as energy per unit area. The hardness, tensile and Charpy-V impact tests were performed at room temperature.

3. Results

3.1. DTA and TGA analyses

Fig. 4 depicts the transformation temperatures (A1 and A3) of the samples determined by DTA analysis. The red arrows show

Fig. 2. The casting processes and the rolled products (a) ceramic molds, (b) heating of ceramic molds, (c) casting process, (d) as-casted steel, (e) hot rolled steels.

Table 1
The chemical composition of the as-cast steels (in wt. %).

Alloy	C	Cr	W	V	Si	Mn	Ta	N	O	Co
3 Cr-3W-0 Co	0.01–0.07	2.94–3.08	2.95–3.22	0.23–0.29	0.08–0.11	0.33–0.49	0.1	0.017–0.018	0.025–0.038	0
3 Cr-3W-0.5 Co										0.5
3 Cr-3W-1.5 Co										1.5
3 Cr-3W-3 Co										3
3 Cr-3W-4.5 Co										4.5
5 Cr-3W-0 Co	0.04–0.07	4.60–4.87	2.85–3.07	0.23–0.25	0.19–0.28	0.40–0.48	0.1	0.018–0.020	0.024–0.041	0
5 Cr-3W-0.5 Co										0.5
5 Cr-3W-1.5 Co										1.5
5 Cr-3W-3 Co										3
5 Cr-3W-4.5 Co										4.5

A1 and A3 transformation temperatures determined during heating, respectively [13]. A1 and A3 temperatures increased of both alloys (3 Cr and 5 Cr) with an increase in the amount of Co in the alloys. When comparing of transformation temperatures of 3 Cr and 5 Cr alloys according to the amount of Cr, A1 temperature decreased slightly, and A3 temperature increased slightly.

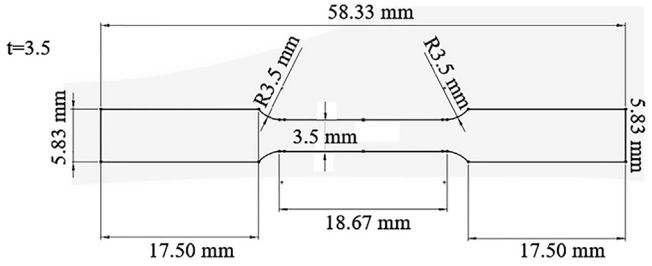

Fig. 3. Schematic diagram of tensile test specimen.

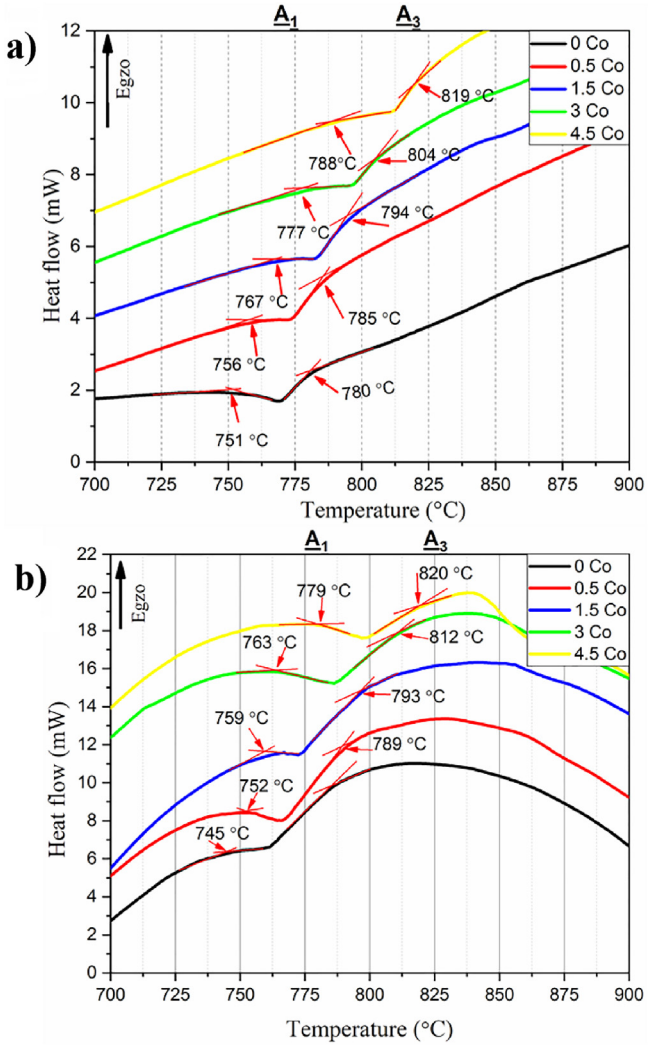

Fig. 4. DTA graphics of (a) 3 Cr alloys, (b) 5 Cr alloys.

Curie temperatures of the samples were also determined by TGA analysis. Fig. 5 shows Curie temperatures changing with an increase in the amount of Co. The rise in the amount of Cr of the alloys, which have the same amount of Co, caused to decrease in Curie temperature slightly.

3.2. Optical microstructure examinations

The optical microscope images of the annealed and air-cooled samples etched using LePera colored etchant agent are given in Figs. 6 and 7. It is impossible to recognize tempered bainite and tempered martensite with the optical microscope after tempering.

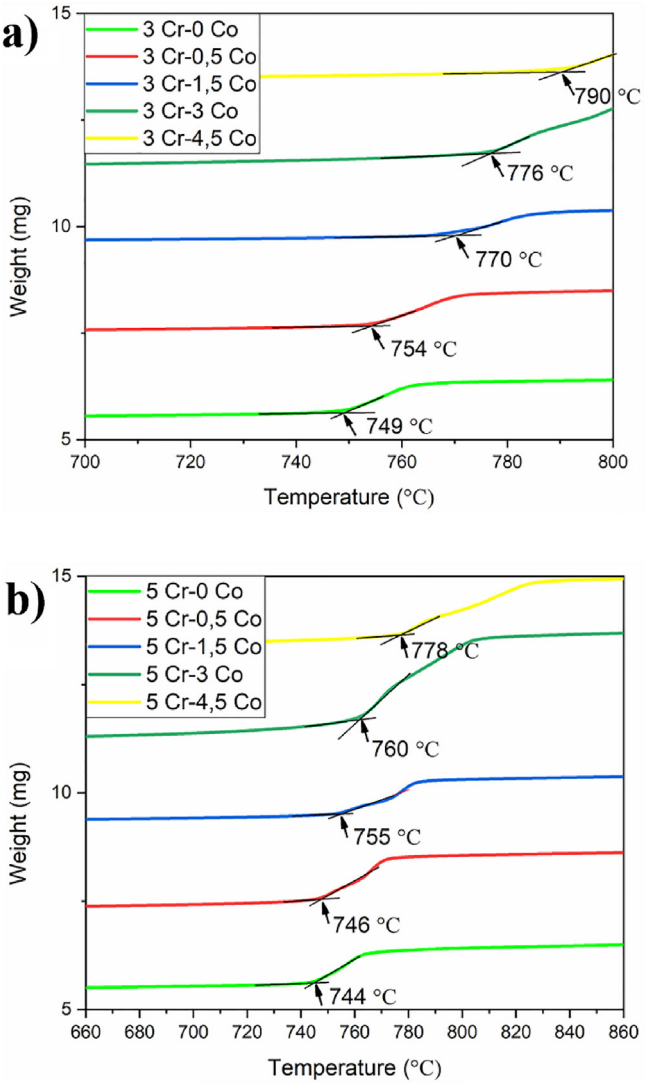

Fig. 5. Curie temperatures of (a) 3 Cr alloys, (b) 5 Cr alloys.

Therefore, the current phases in the microstructure were examined before tempering. While there is no martensite in microstructures of 3 Cr alloys, the phase (white areas [14,15]) can be seen in 5 Cr alloys. The amount of martensite phase decreases with an increase in the amount of Co. The bainite and ferrite phases are observed in the microstructure of 3 Cr-4.5 Co alloy are indicated in the Fig. 6 (f) and bainite and martensite phases are observed in the microstructure of 5 Cr-0 Co alloy are indicated in the Fig. 7 (f) as well as the color etching is done to indicate the martensite phases.

The optical microscope images of the annealed, air-cooled and then tempered samples etched with picral are given in Figs. 8 and 9.

Ferrite and tempered bainite phases are observed in the microstructure of 3 Cr steel after heat treatment (Fig. 8). Allotriomorphic ferrite precipitated at the grain boundaries, bainitic ferrite extending into the grain, and prior austenite grain boundaries are encountered in 3 Cr alloys. However, the amount of ferrite goes up in the alloy containing 4.5% Co. The phases and prior austenite grain boundaries are observed in microstructure of 3 Cr-0 Co alloy are indicated by arrows in Fig. 8 (f). The image of 3 Cr-0 Co alloy has been zoomed and the color of image has been changed to make it look better.

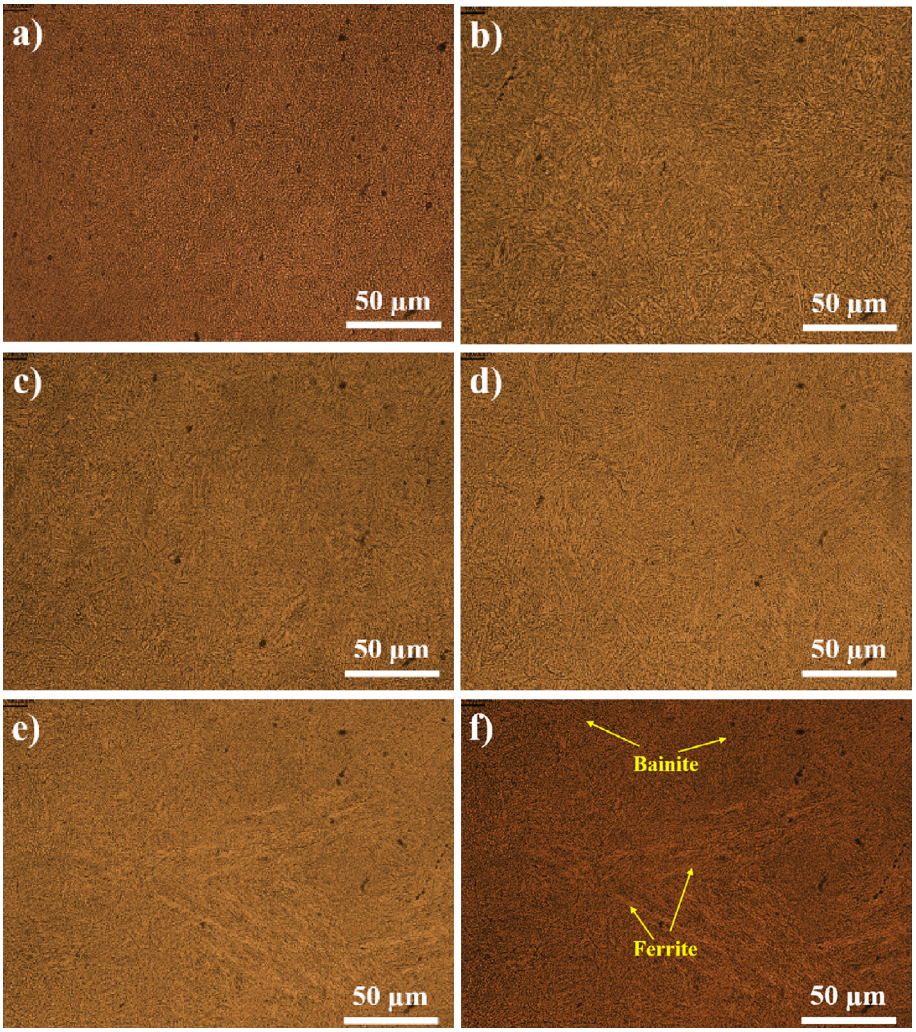

Fig. 6. The optical microscope images of the annealed and air-cooled 3 Cr alloys etched using Lepera agent (a) 0 Co, (b) 0.5 Co, (c) 1.5 Co, (d) 3 Co, (e) 4.5 Co, (f) 4.5 Co.

Tempered bainite and tempered martensite phase are observed in the microstructure of 5 Cr steel after heat treatment (Fig. 9). Bainitic ferrite placed into the grain, and prior austenite grain boundaries are encountered in 5 Cr alloys. The phase and prior austenite grain boundaries are observed in microstructure of 5 Cr-0 Co alloy are indicated by arrows in Fig. 9 (f). The image of 5 Cr-0 Co alloy has been zoomed and the color of image has been changed to make it look better.

Table 2 shows the volume fraction of ferrite phase in 3 Cr alloys. The first addition of Co decreases volume fraction of ferrite but ferrite phase increased, especially, after more than 3% Co addition.

3.3. SEM examinations

The SEM images of the annealed and tempered 3 Cr and 5 Cr samples are given in Figs. 10 and 11, respectively. Prior austenite grain boundaries, bainitic lath boundaries, precipitated particles at the grain boundaries, and into the grain can be easily observed in SEM images of alloys.

3.4. SEM-EDS analyses

The chemical composition of the matrix phase and the particles precipitated into the grain and grain boundaries after heat treatments were determined by SEM-EDS line and point analyses (Figs. 12 and 13). It was observed that the content of the carbide-forming elements such as Cr, W, Ta are high in the precipitates.

3.5. TEM examinations

Precipitates obtained by carbide extraction were examined with TEM. The TEM image of precipitates of 5Cr-3W-1,5Co alloy is shown in Fig. 14. Dimensional and morphological evaluation of the precipitates was carried out. It can be mentioned from the TEM images that the carbides formed in different sizes and morphology.

3.6. TEM-EDS analyses

Fig. 15 shows the image of the TEM-EDS surface analysis. In the analyses, black and white images represent the regions that are analyzed, and colored areas represent the elements in these regions. Table 3 provides the amounts of the elements obtained from TEM-EDS analysis.

3.7. XRD analyses

XRD analyses were performed on the precipitates obtained by carbide extraction. The results of the XRD analysis of 3

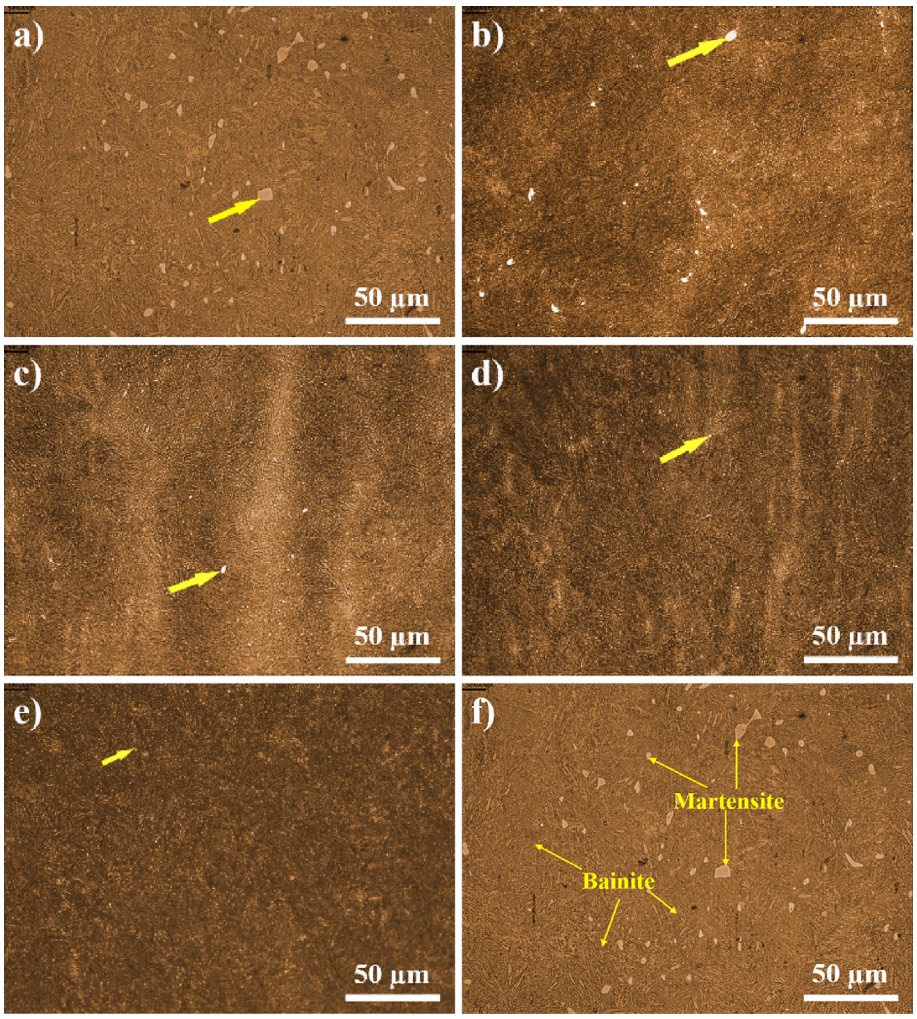

Fig. 7. The optical microscope images of the annealed and air-cooled 5 Cr alloys etched using Lepera agent (a) 0 Co, (b) 0.5 Co, (c) 1.5 Co, (d) 3 Co, (e) 4.5 Co, (f) 0 Co.

Cr and 5 Cr alloys are given in Figs. 16 and 17, respectively. XRD analysis was performed for the identification of precipitates formed. At the same time, it was identified whether XRD graphics change depending on the amount of Co and Cr of alloys.

According to XRD analysis results, it is observed that alloy carbides and nitrides are formed in the microstructure. The increase in peak intensity is observed due to the increase in Co amount in 3 Cr and 5 Cr alloys. It is seen that the peak intensity is increased by increasing the amount of Cr in alloys that have the same amount of Co.

3.8. Hardness tests

The hardness plots of 3 and 5 Cr alloys after both air quenching and air quenching and tempering are shown in Figs. 18 and 19, respectively. It was observed that the hardness of both the 3 Cr and 5 Cr steel was slightly increased with the first addition of Co in both heat treatment conditions (quenching and quenching + tem pering). However, it was seen that the further addition of Co did not increase the hardness considerably. In addition to this, there was a slight decrease in hardness in 3 Cr alloys which have more than 3% Co after tempering.

When the hardnesses of the 3 Cr and 5 Cr alloys are compared, the hardness of the 5 Cr alloys is higher than 3 Cr alloys after quenching, but the hardness of the 5 Cr alloy is lower than 3 Cr alloys after tempering.

3.9. Tensile tests

The tensile and yield strength values of 3 Cr and 5 Cr alloys after air quenching-and tempering are shown in Figs. 20 and 21, respectively. A similar tendency with hardness appears in strength values. The strengths of 3 Cr steels increased with addition up to 3% Co but further Co addition decreased strengths slightly. The strengths of 5 Cr alloys slightly increased and then remained constant with addition of Co. The strength of 5 Cr alloys is generally lower than the 3 Cr alloys.

3.10. Notch impact tests

The impact energies of 3 Cr and 5 Cr alloys after heat treatment (air quenching and air quenching-tempering) are shown in Figs. 22 and 23, respectively.

Although there is a slight decrease in notch toughness of 3 Cr alloys, including up to 1.5% Co and 5 Cr alloys, including up to 3% Co, respectively, they have drastically decreased with further increase of Co Figs. 24 and 25 show the SEM images of fractured surfaces of 3 Cr and 5 Cr alloys, respectively, that were taken to examine the structure of fracture surfaces after impact tests. SEM

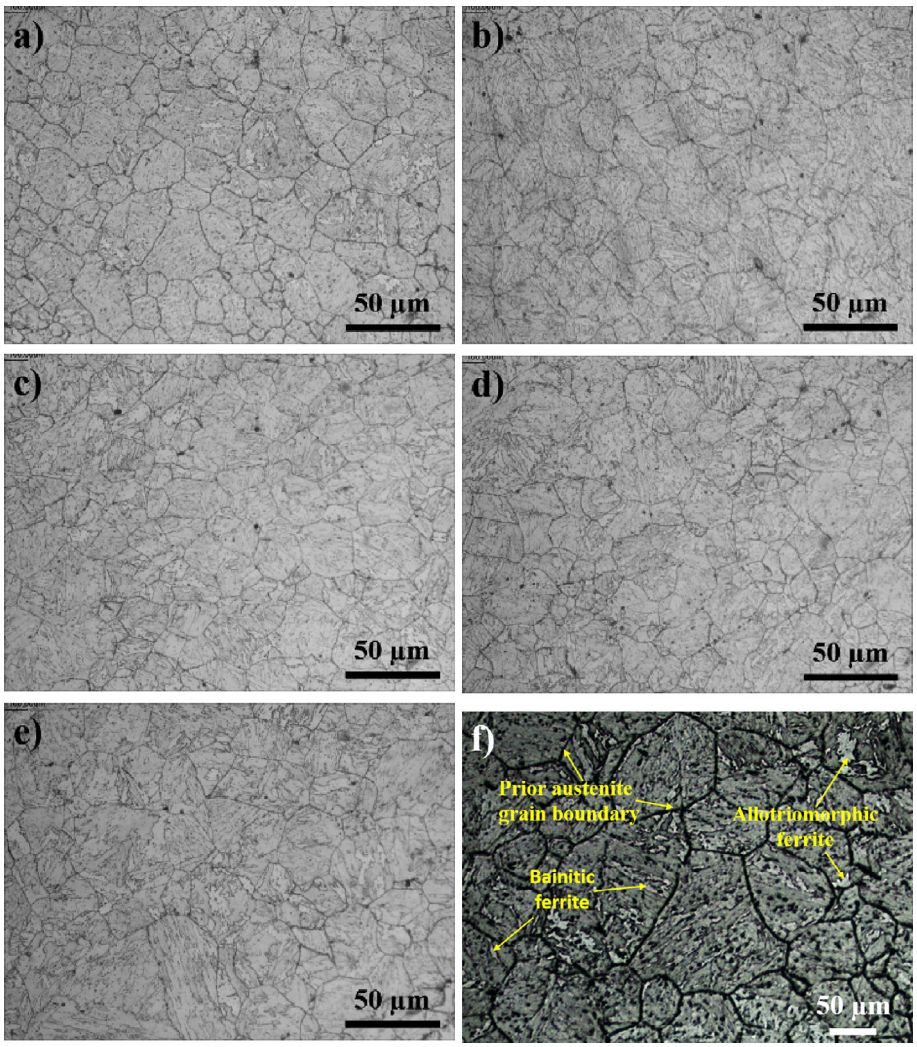

Fig. 8. The optical microscope images of tempered 3 Cr alloys (a) 0 Co, (b) 0.5 Co, (c) 1.5 Co, (d) 3 Co, (e) 4.5 Co, (f) 0 Co.

images of fracture surfaces inform about fracture type (brittle or ductile).

When the fracture surfaces are examined, it can be said that Co-free 3 Cr alloys showed a ductile fracture. When Co is added to the alloy, it is observed that ductile behavior decreased, and brittle fractures occurred.

When the fracture surfaces are examined of 5 Cr alloys, it can be said that Co-free 5 Cr alloys showed an intergranular and transgranular brittle fracture. When further adding of Co to the alloy the brittle behavior continued to be seen. Fracture of 5 Cr alloys, including 4.5% Co showed more intergranular brittle fracture compare to transgranular brittle fracture than other alloys.

EDS point analyses were also carried out to identify inclusions obtained from fracture surfaces after the impact tests.

Fig. 26 shows the result of SEM-EDS analysis and the SEM images of the inclusion of an alloy. The inclusions are rich in elements such as O, Mn, and S.

4. Discussion

4.1. Microstructure characterization

Microstructural changes in both Co-free and Co containing 3 Cr alloys can be explained by the CCT diagram. Co is an element which shifts the CCT diagram to the left [16]. Slowing or accelerating the carbon diffusion in γ lattice by alloying elements, i.e., slowing or accelerating the transformation of $\gamma \rightarrow \alpha$, determines the increase or decrease of the hardenability. Co has an effect that accelerates the $\gamma \rightarrow \alpha$ transformation, which reduces hardenability. Co causes to shift the CCT curve to the left. This mechanism is not completely clear yet, but it is thought that, if the diffusion of the alloy elements into the γ phase is active, this increases entropy during cooling and makes the γ phase stable thermodynamically. Therefore, this effect of alloying element delays the $\gamma \rightarrow \alpha$ transformation, vice versa [17–19].

Tempered bainite and tempered martensite phase are observed in the microstructure of 5 Cr steel after heat treatment. Since Cr is an element that shifts the CCT diagram to the right [19], that is, it increases the hardenability, the ferrite phase, which is observed in 3 Cr alloys, is not observed in 5 Cr alloys. With this effect of Cr, martensite has formed in the microstructure. The critical nose of the CCT curve shifts to the left again when Co is added to the alloy. As a result of shifting of CCT curves to the left, the martensite ratio decreased as a result of less cutting of the martensite region during cooling. It is impossible to identify tempered bainite and tempered martensite with the optical microscope. The variation in the amount of martensite with the addition of Co (Fig. 7) is consistent with Reference [16] and [20].

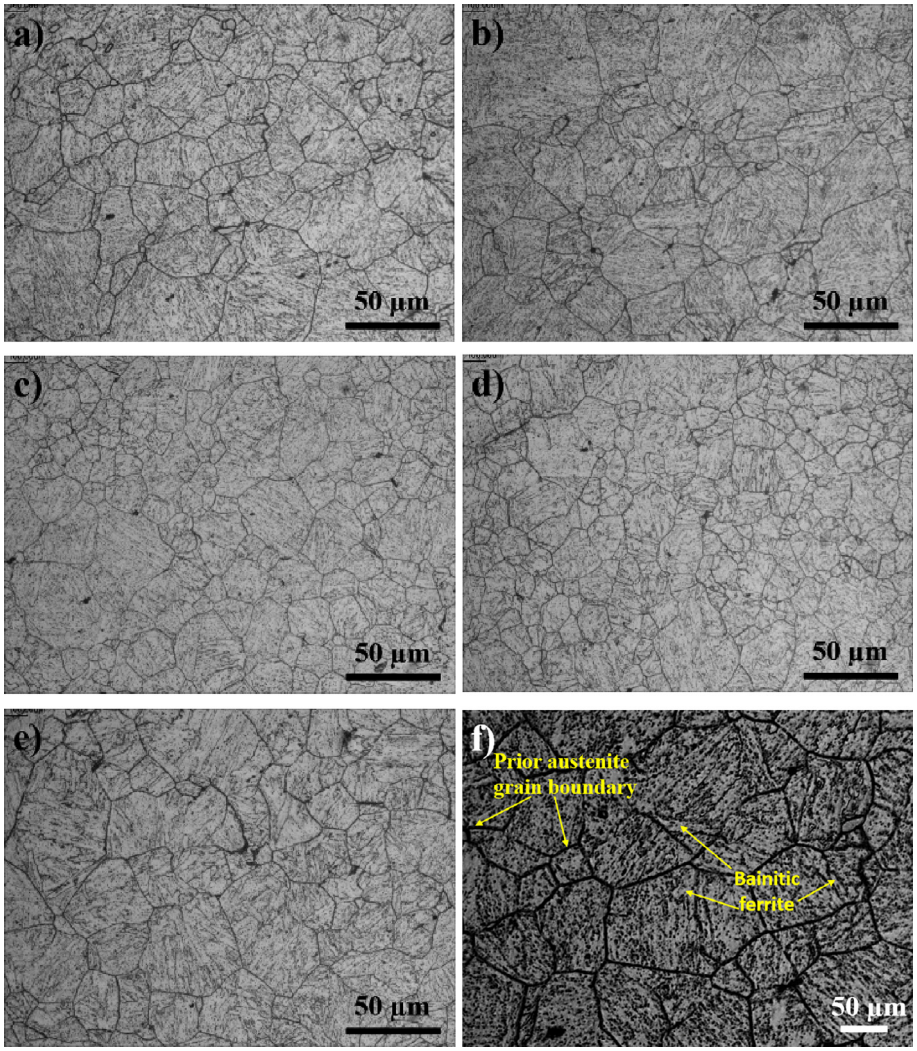

Fig. 9. The optical microscope images of tempered 5 Cr alloys (a) 0 Co, (b) 0.5 Co, (c) 1.5 Co, (d) 3 Co, (e) 4.5 Co, (f) 0 Co.

Table 2
The volume fraction of ferrite.

Alloy	Approximately the volume fraction of ferrite (%)
0 Co	4.59
0.5 Co	1.397
1.5 Co	1.907
3 Co	3.409
4.5 Co	6.167

Co is not a carbide-forming element. However, it promotes the formation of carbides of other metals indirectly. The addition of Co to the alloy increases the density of dislocation in the alloy. As the Co content increases, the dislocation density increases. Increasing of dislocation density acts as sites for nucleation of precipitates and grains. Co indirectly provides refining of grains in this way [21].

The precipitates that can be formed in Cr-Mo (W) steels are carbides, nitrides and Laves phases such as MX, M_2C, M_7C_3, M_3C, $M_{23}C_6$, M_6C, Fe_2Mo and Fe_2W [22–26].

In MX type precipitate, M often represents V, Nb or Ta, and sometimes it represents W; and X represents C or N [27,28]. In M_2C type precipitate, M represents W. In M_3C type precipitate, M generally represent Fe and Cr [28]. Cr can replace by Fe with an increase of tempering time of M_3C type carbide. Depending on the Cr ratio, M_3C type carbides can convert to M_7C_3 and $M_{23}C_6$ type carbides [29]. M_7C_3 type carbides are dominant in alloys, which contain less than 7 wt% Cr. In M_7C_3 type precipitate, M usually represents Fe and Cr [19,30,31].

XRD analysis is used to identify the precipitates which form in alloys. As can be seen from the X-ray diffraction patterns (Figs. 16 and 17), existing precipitates in the structure are carbide and nitride phases. Although there is not much difference in 3 Cr and 5 Cr alloys depending on the amount of Co, the peak intensities increase significantly in the alloy that contains 4.5% Co. The increase of peak intensities can be attributed to Co, which increases carbide activity and promoting carbide formation [7,8]. The peak intensities of carbides in 5 Cr alloys are higher than that of 3 Cr alloys. Although the phases generally formed in alloys are the same, Cr_7C_3 carbide is much more dominant in 5 Cr alloys. Co promotes the formation of ultra-fine and more carbide by increasing C activation. Also, Co reduces the solubility of other elements by dissolving entirely in the Fe matrix, thereby increasing the tendency to precipitate [21]. 3 Cr and 5 Cr alloys, which contain 4.5% Co have ultra-fine and more dispersed precipitate than other alloys. Cr increases the tendency of carbide formation by reducing

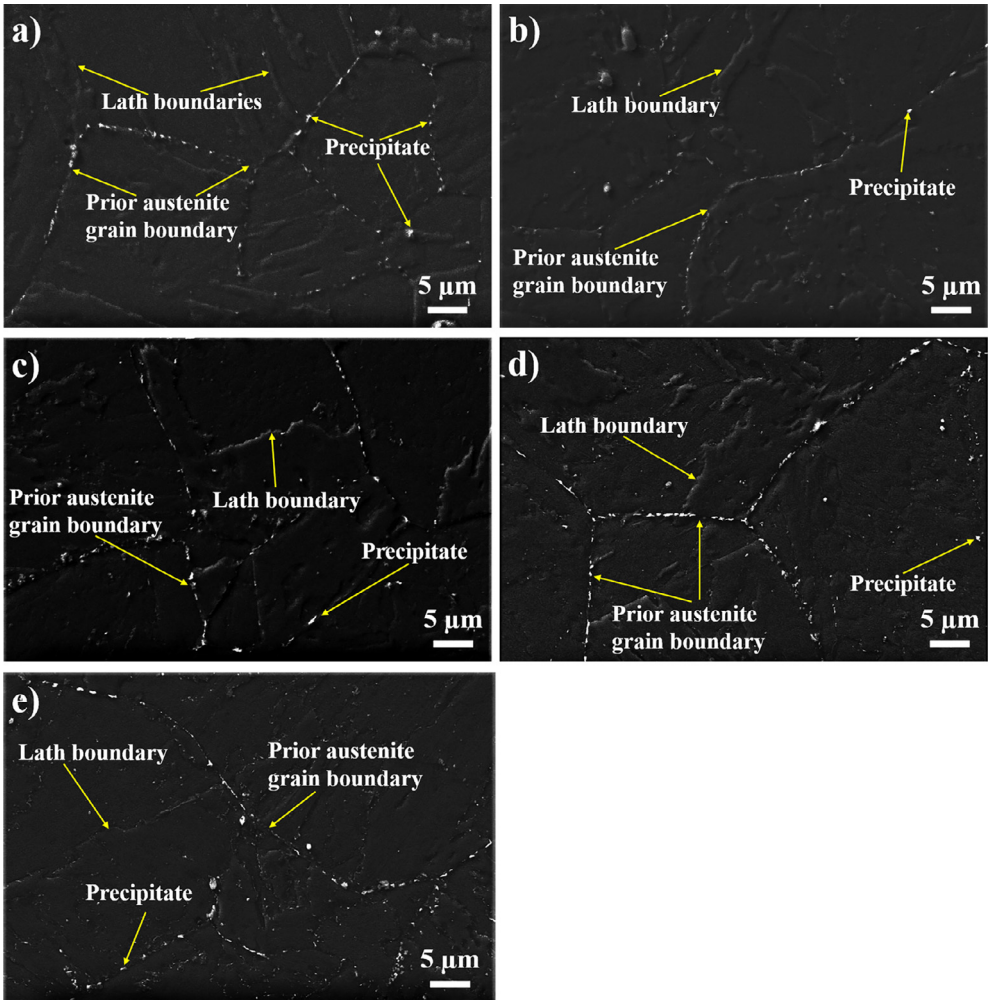

Fig. 10. The SEM images of 3 Cr alloys. (a) 0 Co, (b) 0.5 Co, (c) 1.5 Co, (d) 3 Co, (e) 4.5 Co.

the C that γ-iron can dissolve [19]. SEM-EDS and TEM-EDS analysis results are compatible with the X-ray diffraction patterns of the precipitates that formed in the microstructure.

DTA analysis results show that Co increases the A1 and A3 temperatures. This rise allows austenitization and tempering at higher temperatures, which let the alloying elements dissolve easier in steel and tempering at higher temperatures in a shorter time [32,33]. Since Cr increases the A1 and A3 temperatures and reduces the A4 temperature, it leads to the narrowing of the austenite zone and expanding of the ferrite region [34].

TGA analysis results show that Co increases the Curie temperature. According to the literature, Co is the only alloying element that is known to increase the Curie temperature. The ferromagnetic array below Curie temperature causes a retarding effect on diffusion [9,35]. Co leads to increase the Ms temperature and promotes the precipitation of carbide by retaining the dislocation substructure during tempering, this provides more nucleation sites and a finer dispersion of carbides. [8,9]. Co also increases the bond strength in the iron matrix, promotes the formation of secondary carbides after tempering, and prevents the coarsening of carbides. It is stated that Co increases the activity of C [7,8]. This case contributes to increasing the strength of the material, especially at high temperatures.

4.2. Mechanical properties

Co provides to increase the hardness of steel. Co is not a carbide-forming element, but it helps to increase attainable hardness. Cobalt decreases the stacking fault energy of lattice, which leads to higher dislocation density. Consequently, increasing dislocation density contributes more sites for nucleation and ultra-fine distribution of precipitate [21].

In the study, the carbides that were taken into solution during annealing were precipitated after tempering, and finally, carbide/nitride containing compounds were formed in the microstructure. One of the main aims of tempering is to form these precipitates in the microstructure to improve the mechanical properties, especially high-temperature resistance. Another factor that increases the mechanical properties is solid-solution strengthening provided by alloying elements.

"The addition of Co activates several strengthening mechanisms by reducing the prior austenite grain and subgrain sizes and promoting precipitation within the grains and at their boundaries [36,37]. The hardnesses of both the 3 Cr and 5 Cr steels slightly increased with the first addition of Co in all heat treatment conditions (quenching and quenching + tempering). However, the further addition of Co did not increase the hardness considerably. In

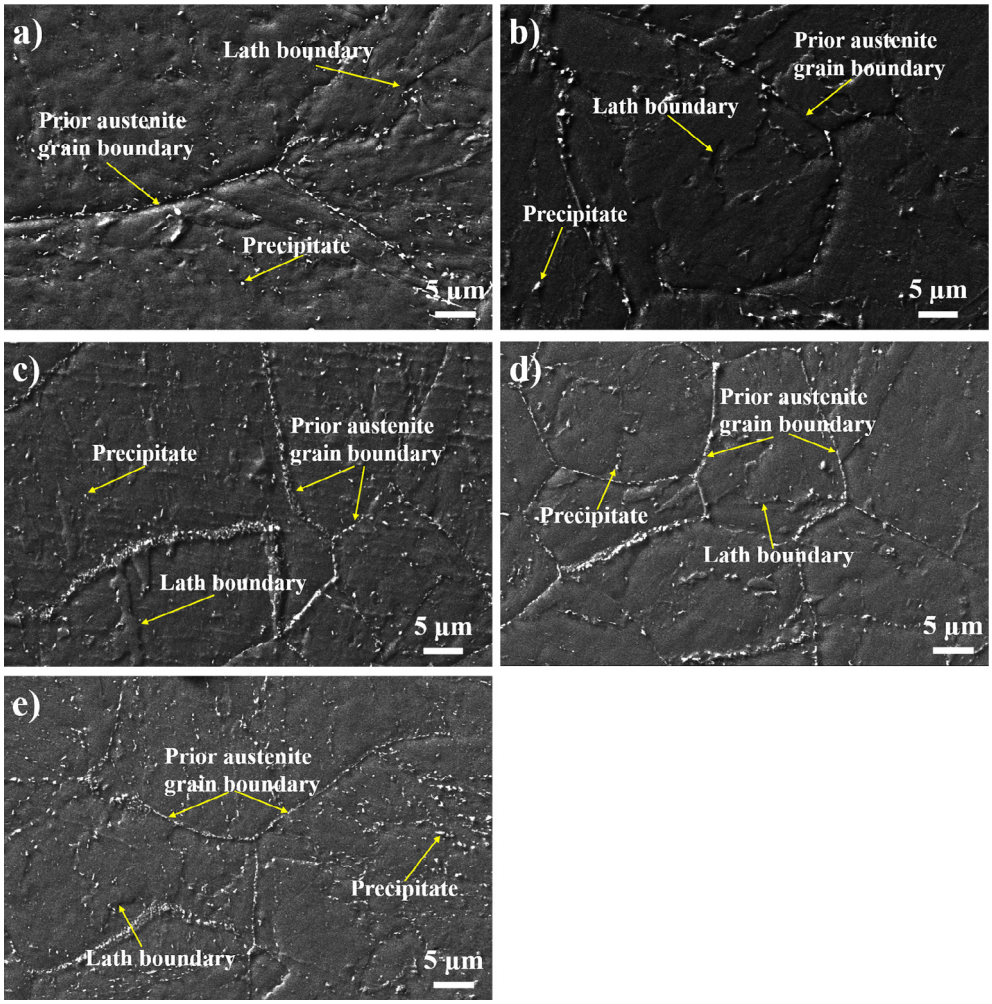

Fig. 11. The SEM images of 5 Cr alloys. (a) 0 Co, (b) 0.5 Co, (c) 1.5 Co, (d) 3 Co, (e) 4.5 Co.

addition to this, there was a slight decrease in hardness in 3 Cr alloys which have more than 3% Co after tempering. This suggests that the reduction in the grain and subgrain size and enhanced precipitate formation are effective in strengthening the low-Cr alloys studied, whereas the solid solution mechanism through Co addition is not effective. This is attributed to the fact that adding up to about 6.3 wt pct Co has a negligible effect on the lattice parameter of iron, which is one of the main factors controlling the solid-solution strengthening [9]. Therefore, unlike W and Mo, Co does not enhance strength through this mechanism. [36,37].

When the hardnesses of the 3 Cr and 5 Cr alloys are compared, the hardness of the 5 Cr alloys is higher than 3 Cr alloys after quenching, but the hardness of the 5 Cr alloy is lower than 3 Cr alloys after tempering. Increasing the amount of Cr in alloys leads to increase the grain size and precipitate size according to literature [38]. More massive carbides are formed in 5 Cr alloys. One reason for the hardness of 5 Cr alloys is lower than the 3 Cr alloys after tempering is: Martensite formed in addition to bainite in 5 Cr alloys. The decrease in hardness on tempering bainite is smaller than martensite because, unlike martensite, there is, in general, little carbon left in solid solution. The martensitic transformation occurs when the carbon atoms do not have the opportunity to diffusion during quenching. Carbon atoms that remain as interstitial transform the structure from face-centered cubic (FCC) to body-centered tetragonal (BCT) by causing the lattice distortion when the quenching rate is rapid enough to prevent diffusion. The hardness of martensite is high as the C atoms prevent the movement of dislocations. Diffusion of C atoms to their normal positions causes to decrease in the hardness of martensite after tempering. The bainitic microstructure contains vigorous carbide forming elements. So, the carbon precipitated as carbides does not cause to decrease in hardness after tempering, unlike martensite [39,40].

The variation of the hardness is parallel to the yield and tensile strengths of 3 Cr and 5 Cr alloys. With the addition of Co to the alloys, the strength increased to a specific rate and then moved horizontally. Co causes a small amount of solid solution strengthening [33]. Some researchers have stated that Co improves the yield strength because it increases the activity of C [21]. With further addition Co more than 3% to 3 Cr alloy decreased strength slightly. The decrease in strength can be attributed to ferrite phase that increased after more than 3% Co addition (Table 2). The volume fraction of ferrite phase was estimated by using image analysis software. Although, the analysis was figured out from 3 different microstructure images, more precise results can be obtained by analyzing from more microstructure images. And the results suggest that the effect of Co on ferrite formation during continuous cooling has not been clearly established because contradictory results can be obtained; therefore, the effect of Co on microstructure in low Cr steels should be further investigated. The strength values increased slightly with addition

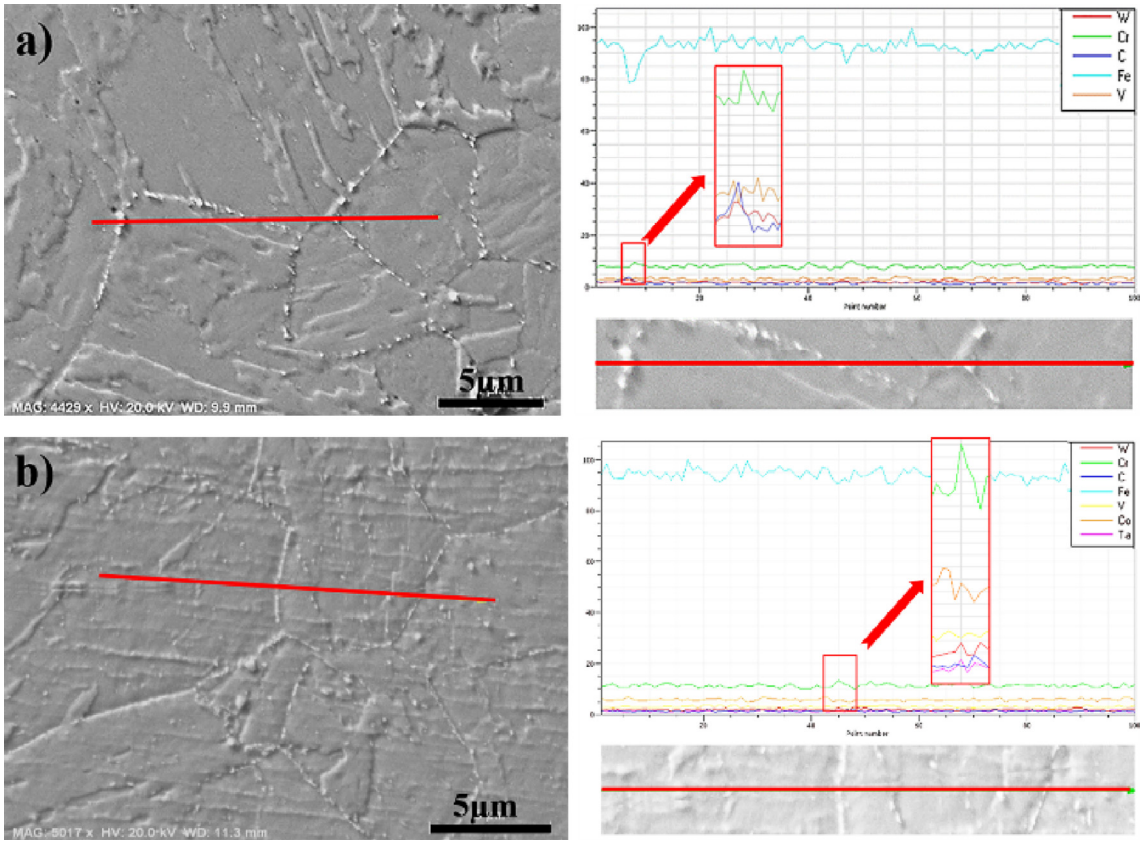

Fig. 12. Result of EDS line scan analyses (a) 3 Cr-0 Co, (b) 5 Cr-3 Co.

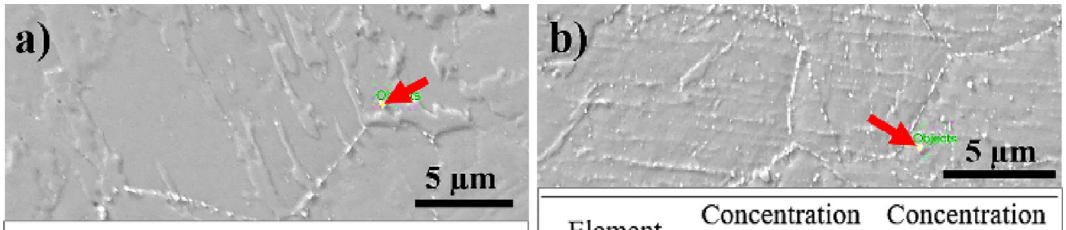

Element	Concentration (wt. %)	Concentration (at. %)
Iron	85.06	86.84
Chromium	4.83	8.30
Tungsten	8.63	2.68
Carbon	0.97	4.62
Vanadium	0.51	0.57

Element	Concentration (wt. %)	Concentration (at. %)
Iron	87.06	87.07
Chromium	5.35	5.73
Tungsten	3.82	1.16
Tantalum	1.04	0.32
Carbon	0.92	4.24
Cobalt	1.23	1.16

Fig. 13. Result of EDS point analyses (a) 3 Cr-0 Co, (b) 5 Cr-3 Co.

of Co to 5 Cr alloys. This condition is similar to that of hardness because martensite loses its strength more than the bainite after tempering [39,40]. After tempering, the strength of 5 Cr alloys was lower than the 3 Cr alloys. This situation is parallel to the hardness values. Possible causes to this reduction is: to decrease in strength during tempering the martensite compared to the bainite [39,40].

The impact energies decrease slightly with increasing Co content up to 1.5% in 3 Cr alloys and up to 3% in 5 Cr alloys, however further addition of Co to the alloys reduce the notch toughness drastically. The addition of Co in ferritic/martensitic steels accelerates the growth of Laves phases, and this leads to intergranular brittle fracture [41]. Birkle and Porter [42] show that the increase of Co content in steel decreases the toughness of the steel. Garrison

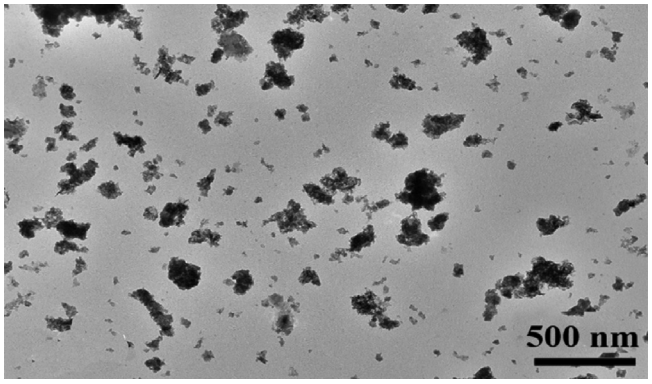

Fig. 14. The TEM image of precipitates of 5 Cr-1.5 Co alloy.

[43] comments that Co has a restrictive effect on grain formation and cross slip, thereby reducing toughness, similar to that obtained by lowering the test temperature. Actually, Laves phase forms in high Cr steel at elevated temperature for a long time. Therefore, in this study, lower toughness of the steels may be caused by effect of Co on slipping.

The notch toughness of 3 Cr alloys is higher than for the 5 Cr alloys. Cr caused to reduce the amount of ferrite and led to martensite formation. For this reason, the structure has become brittle. At the same time, Cr is a carbide-forming element [19] and can, therefore, cause the structure brittle.

When the fractured surfaces of the 3 Cr alloys after the notch impact test are examined with SEM, the surface images up to 3% Co are almost similar. In the alloys containing 3% Co, intragranular brittle fracture took place, and in all other alloys, intergranular brittle breakage came off. In the 5 Cr alloys' fractographs, brittle fracture is observed. The intergranular brittle fracture tends to return to intragranular brittle fracture as the amount of Co

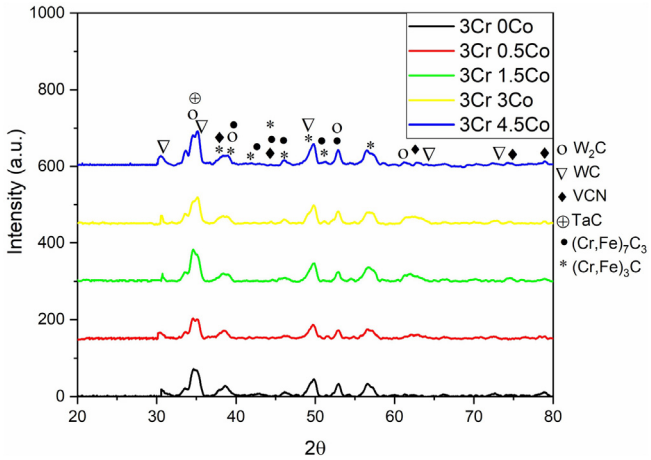

Fig. 16. XRD graphs of carbides formed in 3 Cr alloys.

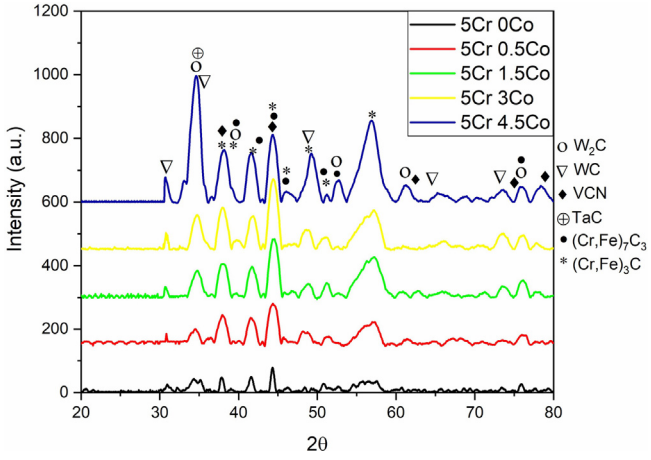

Fig. 17. XRD graphs of carbides formed in 5 Cr alloys.

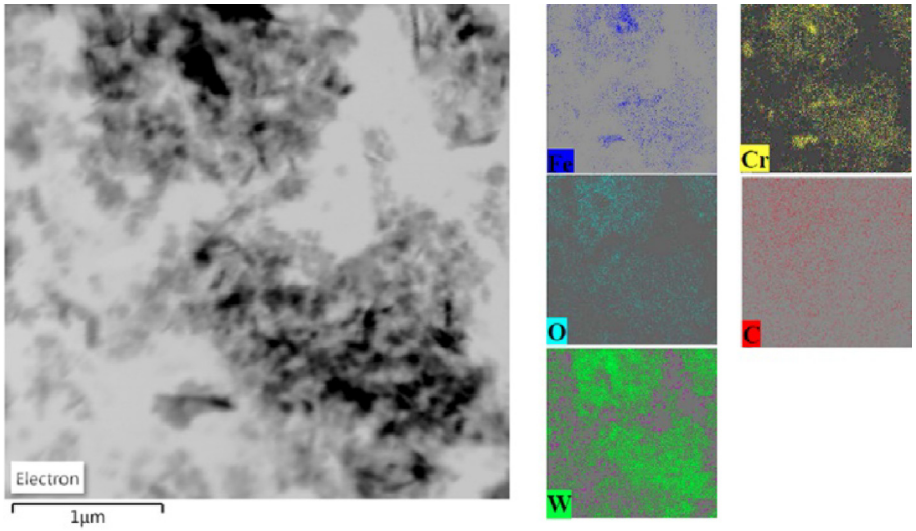

Fig. 15. The image of the TEM-EDS surface analysis of precipitates of 5 Cr-4.5 Co alloy.

Table 3
The elemental distribution of precipitates of 5 Cr-4.5 Co alloy (in wt. %).

Alloy	W	Fe	Cr	V	C	O
5 Cr-3W-4.5 Co	62.36	5.17	5.17	6.64	12.92	7.75

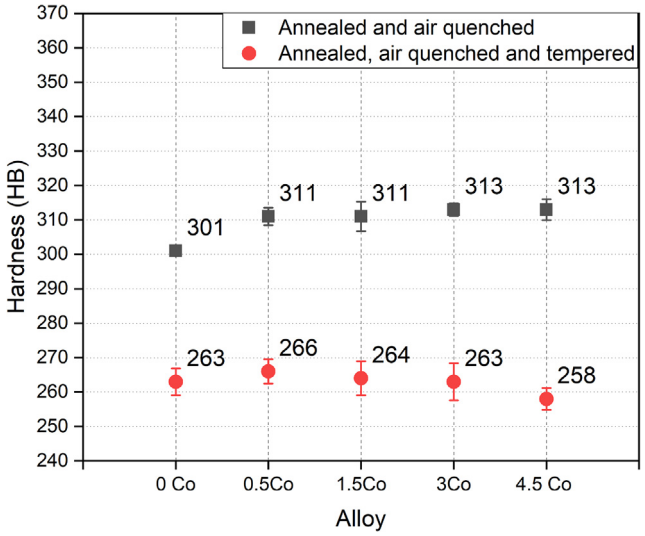

Fig. 18. Hardness values of 3 Cr samples.

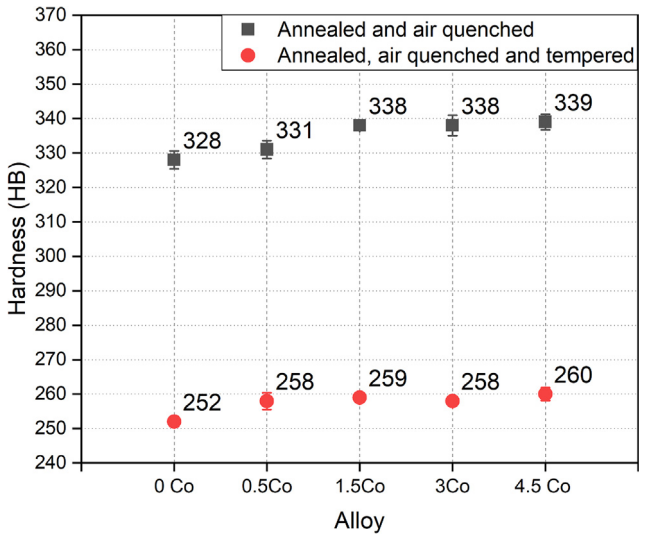

Fig. 19. Hardness values of 5 Cr samples.

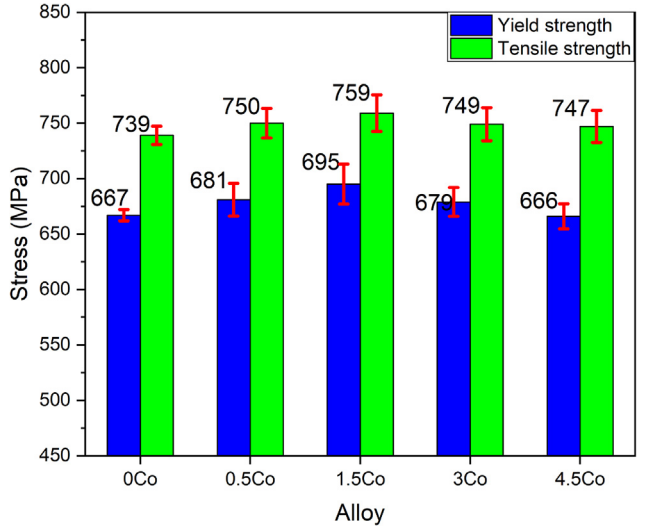

Fig. 20. The yield and tensile strength values of 3 Cr alloys.

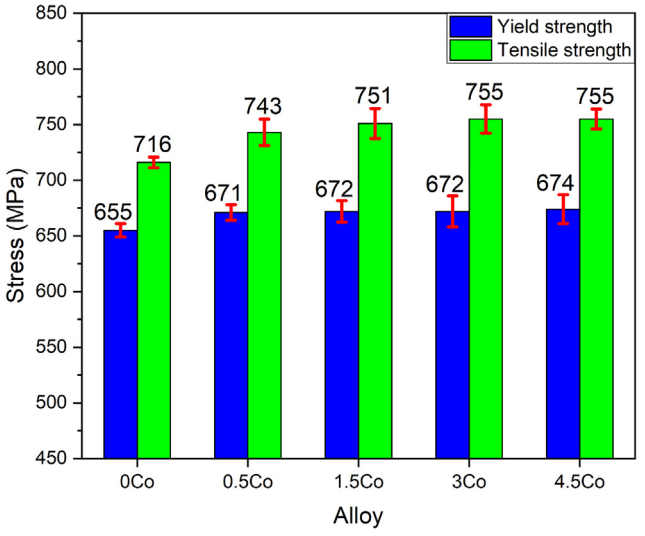

Fig. 21. The yield and tensile strength values of 5 Cr alloys.

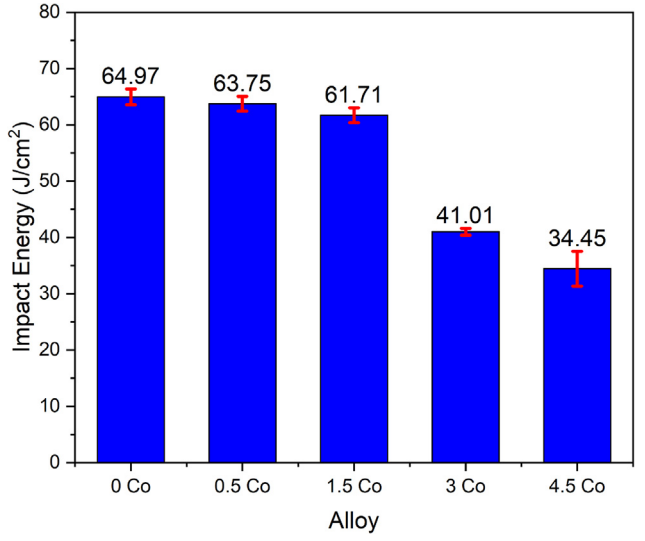

Fig. 22. Notch toughness of 3 Cr alloys.

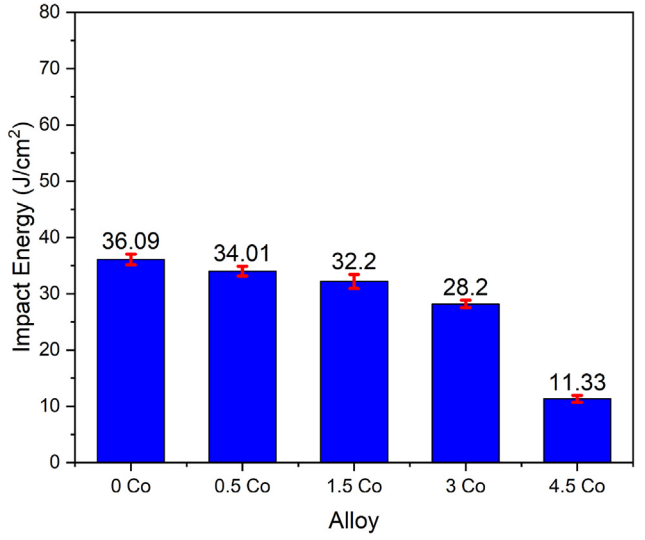

Fig. 23. Notch toughness of 5 Cr alloys.

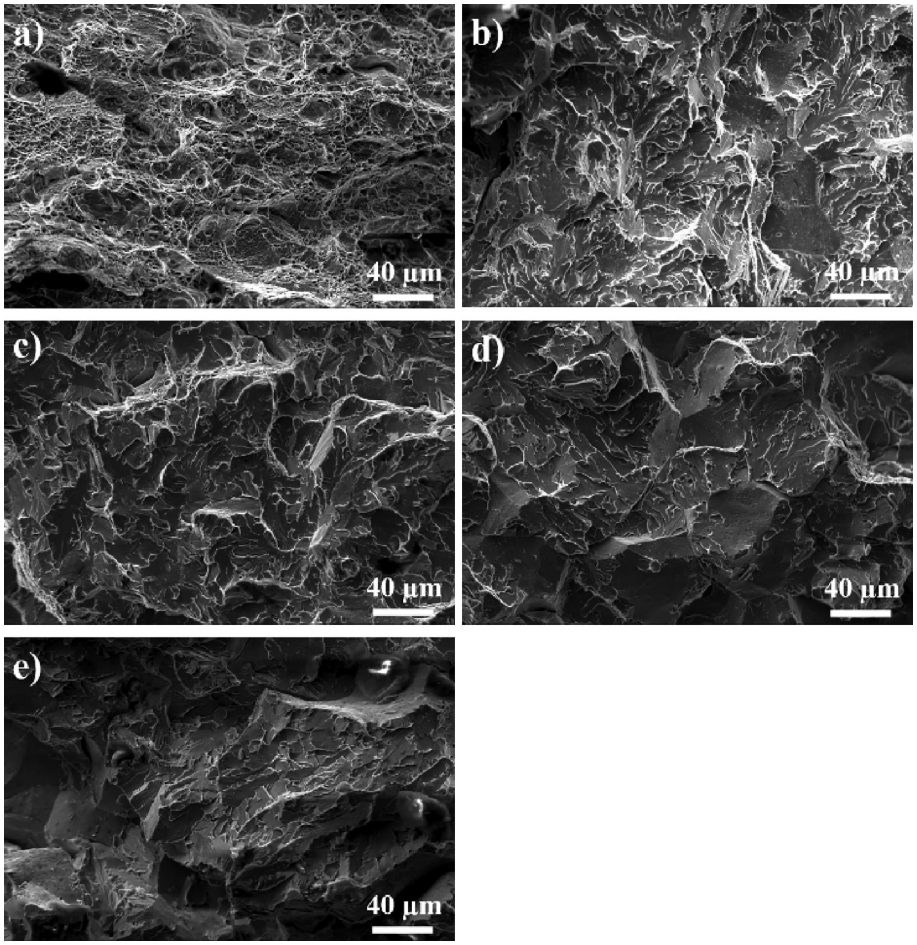

Fig. 24. The SEM images of fracture surfaces of 3 Cr alloys after Charpy impact test (a) 0 Co, (b) 0.5 Co, (c) 1.5 Co, (d) 3 Co, (e) 4.5 Co.

increases. Intergranular fracture is due to brittle phases that formed on grain boundaries.

5. Conclusions

In this study, 3Cr-3W-xCo and 5Cr-3W-xCo alloys fabricated by casting with and without Co were characterized through microstructural observations and mechanical tests. The following conclusions have been drawn.

Depending on the amount of Co, ferrite, and bainite phases are observed in 3 Cr alloys, while bainite and martensite phases are observed in 5 Cr alloys.

With the increase in Co amount, martensite formation decreased in 5 Cr steel while the amount of bainite increased.

A1, A3, and Curie temperatures increased as Co bearing to the 3 Cr and 5 Cr alloys. Carbides/nitrides formed in the microstructure after annealing, air quenching, and tempering heat treatments were observed with SEM, and it was determined by XRD analysis that these precipitates are MX, M_2C, M_3C and M_7C_3.

The addition of Co contributed to the increase of mechanical properties to a certain extent.

Co has a toughness reducing effect.

Declaration of Competing Interest

The authors declare that they have no known competing financial interests or personal relationships that could have appeared to influence the work reported in this paper.

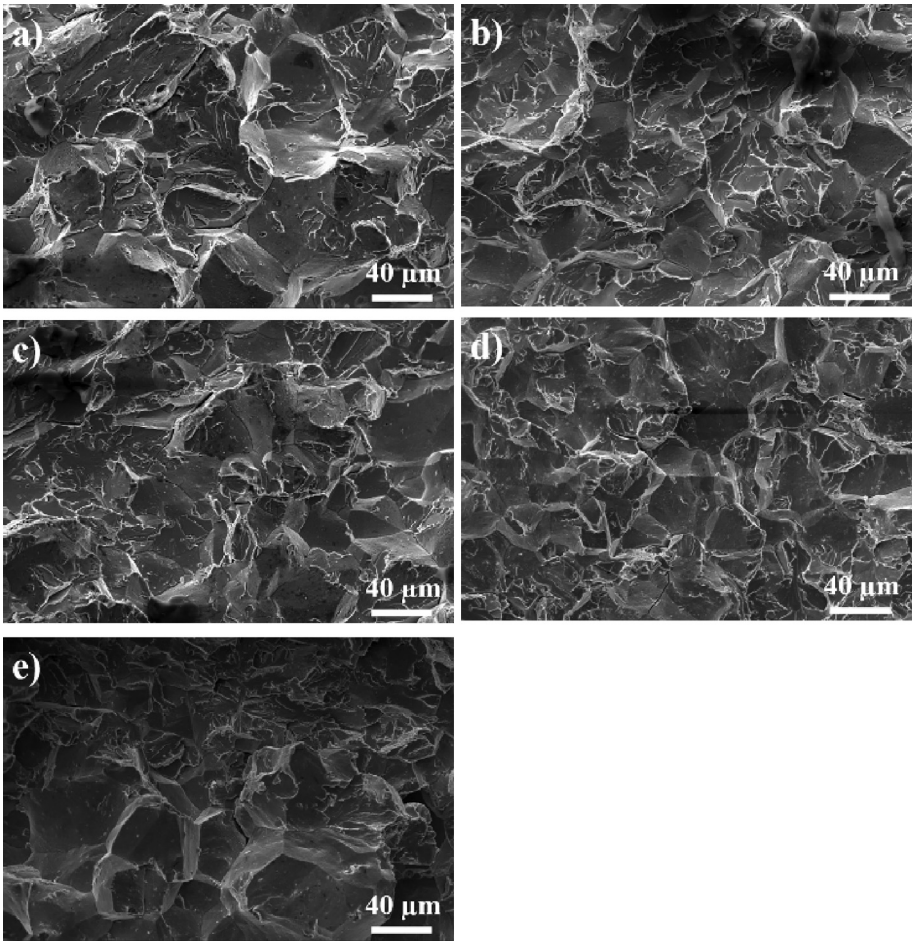

Fig. 25. The SEM images of fracture surfaces of 5 Cr alloys after Charpy impact test (a) 0 Co, (b) 0.5 Co, (c) 1.5 Co, (d) 3 Co, (e) 4.5 Co.

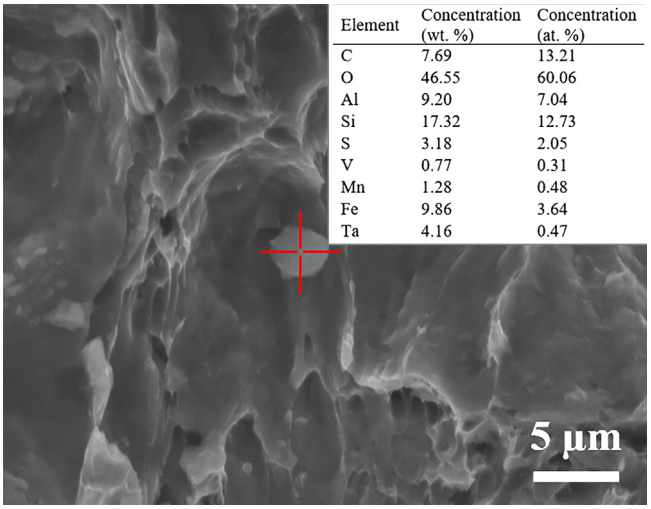

Element	Concentration (wt. %)	Concentration (at. %)
C	7.69	13.21
O	46.55	60.06
Al	9.20	7.04
Si	17.32	12.73
S	3.18	2.05
V	0.77	0.31
Mn	1.28	0.48
Fe	9.86	3.64
Ta	4.16	0.47

Fig. 26. The SEM images and the SEM-EDS results of inclusion in 3 Cr-3 Co alloy.

Acknowledgment

This study was carried out as a Ph.D. thesis by Gökhan ARICI in the Graduate School of Natural and Applied Science at Selcuk University, Konya, Turkey. Selcuk University Scientific Research Projects also supported this work for Grant Number 17101001.

References

[1] R.L. Klueh, Elevated temperature ferritic and martensitic steels and their application to future nuclear reactors, Int. Mater. Rev. 50 (2005) 287–310.
[2] F. Abe, Precipitate design for creep strengthening of 9% Cr tempered martensitic steel for ultra-supercritical power plants, Sci. Technol. Adv. Mater. 9 (2008) 13002.
[3] R.L. Klueh, P.J. Maziasz, D.J. Alexander, A comparison of low-chromium and high-chromium reduced-activation steels for fusion applications, Oak Ridge National Lab. (1996).
[4] M. Jawad, V.K. Sikka, Development of a New Class of Fe-3Cr-W (V) Ferritic Steels for Industrial Process Applications, Nooter Coorporation (2005).
[5] S. Osgerby, Steam turbines: operating conditions, components and material requirements, in: Struct. Alloy. Power Plants, Elsevier, 2014: pp. 22–35.
[6] J. Onoro, Martensite microstructure of 9–12% Cr steels weld metals, J. Mater. Process. Technol. 180 (2006) 137–142.
[7] A.P. Gulyaev, I.K. Kupalova, Effect of cobalt on the structure and properties of high-speed steels, Met. Sci. Heat Treat. 12 (1970) 666–671.
[8] R. Viswanathan, W. Bakker, Materials for ultrasupercritical coal power plants—Boiler materials: Part 1, J. Mater. Eng. Perform. 10 (2001) 81–95.
[9] A. Magnee, J.M. Drapier, D. Coutsouradis, L. Habrakan, J. Dumont, Cobalt monograph series: Cobalt-containing high-strength steels, Centre d'Information Du Cobalt, Belgium, 1974.
[10] E. Saikoff, E. Andersson, F. Bengtsson, C. Olausen, M. Galstyan, D. Vikström, J. Lazraq Byström, Cobalt in high speed steels, (2018).
[11] R. Viswanathan, Advances in materials technology for fossil power plants: Proceedings from the fifth international conference, october 3-5, 2007, marco island, florida, USA, ASM International, 2008.
[12] J. Obiko, L.H. Chown, D.J. Whitefield, Microstructure characterisation and microhardness of P92 steel heat treated at the transformation temperatures, in: IOP Conf. Ser. Mater. Sci. Eng., IOP Publishing, 2019: p. 12014.
[13] M. Gojić, M. Sućeska, M. Rajić, Thermal analysis of low alloy Cr-Mo steel, J. Therm. Anal. Calorim. 75 (2004) 947–956.
[14] EWI, Martensite and Bainite in CGHAZ of HSLA Steel Welds, 2020 (2015). https://ewi.org/martensite-and-bainite-in-cghaz-of-hsla-steel-welds/.
[15] E.V. Morales, I.S. Bott, R.A. Silva, A.M. Morales, L.F.G. de Souza, Characterization of carbon-rich phases in a complex microstructure of a commercial X80 pipeline steel, J. Mater. Eng. Perform. 25 (2016) 2736–2745.
[16] V. Raghavan, Physical metallurgy: principles and practice, PHI Learning Pvt. Ltd. (2015).
[17] R.A. Grange, Estimating the hardenability of carbon steels, Metall. Trans. 4 (1973) 2231–2244.
[18] H. Bhadeshia, Martensite and bainite in steels: transformation mechanism & mechanical properties, Le J. Phys. IV. 7 (1997) C5-367-C5-376.
[19] G.E. Totten, Steel heat treatment: metallurgy and technologies, CRC press, 2006.
[20] H.K.D.H. Bhadeshia, Mechanical properties of martensite in heat-resistant steels, National Research Institute for Metals, Tsukuba, Japan, 2000.
[21] ich, D.S. Dabkowski, L.F. Porter, Strength and toughness of Fe-10Ni alloys containing C, Cr, Mo, and Co, Metall. Trans. 4 (1973) 303–315.
[22] K. Tamaki, J. Suzuki, Precipitation of carbides during tempering of Cr-Mo steels, Res. Reports Fac. Eng. Mie Univ. (1982) 39–52.
[23] F. Abe, H. Araki, T. Noda, M. Okada, Microstructure and toughness of C-W and Cr-V ferritic steels, J. Nucl. Mater. 155 (1988) 656–661.
[24] J. Janovec, M. Svoboda, A. Výrostková, A. Kroupa, Time–temperature–precipitation diagrams of carbide evolution in low alloy steels, Mater. Sci. Eng. A. 402 (2005) 288–293.
[25] G. Golański, P. Wieczorek, Precipitation of carbides in Cr – Mo – V cast steel after service and regenerative heat treatment, Arch. Foundry Eng. 9 (2009) 97–102.
[26] H. Wang, C. Somsen, G. Eggeler, E. Detemple, Carbide types in an advanced microalloyed bainitic/ferritic Cr–Mo Steel–TEM observations and thermodynamic calculations: Karbide in einem mikrolegierten bainitisch-ferritischen Cr–Mo-Stahl–TEM Charakterisierung und thermodynamische Berechnungen, Materwiss. Werksttech. 49 (2018) 726–740.
[27] R.L. Klueh, P.J. Maziasz, The microstructure of chromium-tungsten steels, Metall. Trans. A. 20 (1989) 373–382.
[28] Dawson, K., Dissimilar metal welds, Ph.D, University of Liverpool, 2012.
[29] M. Nurbanasari, P. Tsakiropoulos, E.J. Palmiere, A study of carbide precipitation in a H21 tool steel, ISIJ Int. 54 (2014) 1667–1676.
[30] R. Jayaram, R.L. Klueh, Microstructural characterization of 5 to 9 pct Cr-2 pct WV-Ta martensitic steels, Metall. Mater. Trans. A. 29 (1998) 1551–1558.
[31] A. Kamble, V. Kulkarni, A Text Book of Metallurgy: Properties and Applications of Ferrous and Non-ferrous Alloys, Harshal Publications, 2017.
[32] B.P. Sharov, V.N. Zikeev, Effect of cobalt on the structure and properties of steel 18Kh2N4MA, Met. Sci. Heat Treat. 19 (1977) 265–268.
[33] R.L. Klueh, N. Hashimoto, M.A. Sokolov, Effect of heat treatment and tantalum on microstructure and mechanical properties of Fe-9Cr-2W-0.25V Steel, in: M. L. Grossbeck, T.R. Allen, R.G. Lott, A.S. Kumar (Eds.), Eff. Radiat. Mater. 21st Int. Symp., ASTM International, West Conshohocken, PA, 2004: pp. 376–390. https://doi.org/10.1520/STP11241S.
[34] T. Arai, G. Baker, C. Bates, B. Becherer, ASM Handbook, Vol. 4: Heat Treating, ASM Int. (1991) 448.
[35] F. Abe, T.-U. Kern, R. Viswanathan, Creep-resistant steels, Elsevier, 2008.
[36] W. Yan, W. Wang, Y.-Y. Shan, K. Yang, Microstructural stability of 9–12%Cr ferrite/martensite heat-resistant steels, Front. Mater. Sci. 7 (2013) 1–27, https://doi.org/10.1007/s11706-013-0189-5.
[37] F. Masuyama, ISIJ Int. 41 (2001) 612–625, https://doi.org/10.2355/isijinternational.41.612.
[38] J.F. da Silva Filho, C.A.S. de Oliveira, N. Fonstein, O. Girina, F.J.F. Miranda, J. Drumond, E.A. Serafim, C.R.M. Afonso, Effect of Cr additions on ferrite recrystallization and austenite formation in dual-phase steels heat treated in the intercritical temperature range, Mater. Res. 19 (2016) 258–266.
[39] H. Bhadeshia, Bainite in Steels, Transformations, Microstructure, and Properties, IOM Communications, Ltd, (2001).
[40] W.D. Callister, D.G. Rethwisch, Materials science and engineering, John wiley & sons NY, 2011.
[41] P. Hu, W. Yan, W. Sha, W. Wang, Z. Guo, Y. Shan, K. Yang, Study on Laves phase in an advanced heat-resistant steel, Front. Mater. Sci. China. 3 (2009) 434.
[42] A.J. Birkle, L.F. Porter, The Effect of Cobalt On the Strength and Toughness of Ni-Cr-Mo High-Yield-Strength Steels, United States Steel Corp. Monroeville PA, 1964.
[43] W.M. Garrison, Cobalt and the Toughness of Steel, in: Mater. Sci. Forum, Trans Tech Publ, 2012: pp. 3–10.